NCBP1 electrophilic-stress signaling in the nucleus promotes alternatively-spliced S6K1 that dominantly inhibits global translation.

Dalu Chang[‡,¶], Mahdi Assari[‡,¶], Chananya Suwathep[†], Khomkrit Sappakhaw[†],

Chayasith Uttamapinant[†], Marcus. J. C. Long[§,¶], and Yimon Aye[‡,¶]

[‡]Swiss Federal Institute of Technology Lausanne (EPFL), Lausanne 1015, Switzerland

[†]Vidyasirimehdi Institute of Science and Technology (VISTEC), Rayong 21210, Thailand

[§]University of Lausanne (UNIL), Epalinges 1066, Switzerland

[¶]NCCR Chemical Biology and University of Geneva, Geneva 1211, Switzerland

Primary contact: yimon.aye@epfl.ch

Abstract

Proteome synthesis is profoundly influenced by subcellular stress. However, both the nature of spatiotemporally-restricted cues and the underpinning local responders mediating these cues remain elusive. Unlocking these mechanisms requires an ability to functionally map in living cells locale-specific stress responders and simultaneously interrogate how a localized cue on specific local players contextually impacts proteome synthesis *in trans*. Here we resolve this prime problem by integrating precision localized electrophile delivery and genetic-code-expansion-based translation reporter tools. Among the four distinct subcellular locales examined, nuclear-targeted stress most prominently inhibits protein translation. We discovered that NCBP1—a nuclear-resident protein with multifaceted roles in eukaryotic mRNA-biogenesis—propagates this nuclear stress signal through a single cysteine (C436) among the 19 conserved, affecting 200 alternative-splicing events across 119 genes differentially-expressed in response to nuclear stress. Global protein-synthesis stall was choreographed by electrophile-labeled NCBP1(C436) triggering the production of alternatively-spliced S6-kinase, which we found to dominantly suppress protein translation.

The canonical protein code contains 20 amino acids, equipping nascent proteins with a battery of reactive, hydrophobic, acidic/basic, and hydrophilic groups that, when positioned accordingly, can perform awesome feats. Some of the examples include proteolysis (e.g., serine, histidine, aspartate catalytic triads), sigmatropic shifts, and redox relays. In combination with cofactors, more possibilities occur, such as decarboxylation and proton-coupled electron transfer. Despite so much being possible with the basic building blocks of life, the pressures of selection have frequently forced nature to accessorize the canonical amino acids. These embellishments occur classically in the form of posttranslational modifications (PTMs)[1]—covalent modifications to specific amino acids within specific proteins that change chemical properties, fundamentally altering regulatory modes, and oftentimes, function.

Numerous efforts have been put into decoding PTM-signaling modes at the pathway and protein-specific levels, giving way to the ubiquitin code, the histone code, and our understanding of phosphosignaling networks. These signals implicate themselves—often in a synergistic manner—in almost all processes in cells. Such regulatory understanding has, in turn, had important ramifications on drug design, disease etiology, and myriad health-related frontiers. Indeed, all the above PTMs are enacted by specific proteins, often referred to as ´writers´, that code these modification-specific signals. These messages are, in turn, interpreted by specific downstream proteins, often referred to as ´readers´. Such a system is clearly an extension of the logic of biochemistry that began with initial forays into understanding enzyme catalysis outlined above. However, over the years, another PTM-driven signaling paradigm has arisen, whereby functional signaling occurs when electrophilic small-molecule metabolites—without the involvement of specific writer proteins—covalently label specific proteins[2-4].

A protein's intrinsic electrophile reactivity and the signaling consequences of electrophile-driven PTMs on proteins, are still mostly unpredictable. Yet, several pathways have emerged to be responsive to non-enzyme-assisted PTMs orchestrated by innate small-molecule electrophiles, oftentimes resulting in dominant loss-of-function signaling consequences through inhibition of a specific POI function/activity. Examples include Akt3 kinase signaling, transcription, antioxidant response and mitochondria-associated programmed cell death[5-7]. Nevertheless, despite our burgeoning attempts to decode this non-canonical form of PTM-signaling, there remain scant paradigmatic examples. This point is magnified particularly in terms of locale-specific sensing, and how specific localized reactive chemical signal inputs are propagated along specific pathways involving defined mediators, leading to functional biological outputs, even at low electrophile occupancy on a single electrophile-sensor protein upstream.

Notably, among the limited instances of biological processes directly influenced by such locale-specific substoichiometric electrophile sensing and signaling, protein translation remains a largely unexplored arena. This is despite the emerging phenomenon surrounding dynamical changes in translation efficiency in response to localized subcellular stress[8,9]. Here, we use an unbiased proteome-wide screen to identify novel locale-specific electrophilic-stress responders, in tandem with a genetic-code expansion[10]-based translation reporter platform. The approach identifies NCBP1 as a novel sensor of the native electrophilic lipid-derived metabolite, 4-hydroxynonenal (HNE). Despite numerous cysteines within NCBP1 capable of competitively sensing HNE, HNEylation only through one specific site (C436) downregulates translation, via deregulating splicing of a number of genes. One of the genes so affected is S6K1, which forms a new isoform, S6K1-X. This protein is dominant negative for translation when expressed in the cell. This event explains the majority of HNEylated NCBP1-induced translation inhibition, as well as how C436-specific HNEylation of primarily nuclear-resident protein NCBP1 impairs translation. We thus provide in detail one of the first examples of a specific protein—electrophile labeling event governing translation efficiency, and a particularly intricate molecular mechanism of translation regulation that proceeds through a gain-of-function splicing event mediated through NCBP1-electrophile labeling. These data overall display the huge richness of reactive small-molecule signaling, and highlight the unpredictability of these important non-canonical PTM signaling events.

RESULTS.

Nuclear-targeted electrophile delivery selectively suppresses global protein synthesis.

To cast a new lens over how localized small-molecule stressors reprogram translation, we set out to unite our recently-developed function-guided proximity mapping (Localis-REX)[6] and the established genetic code expansion (GCE)-based translation reporter system[10,11] (**Fig. 1A**). Localis-REX enables controlled delivery of reactive electrophiles of defined chemotype to a specific locale (organ/cell-type, organelle, subcellular locale, etc.) in cells/animals, with high spatiotemporal resolution (**Supplemental Fig. S1A**). GCE translation reporters give highly-sensitive means to measure dynamic changes in translation (**Supplemental Fig. S1B**). Here we fused Halo to four distinct localization sequences, NLS, NES, MOMLS, and ERt (**Supplemental Table S1-S2**), directing Halo, respectively, to the cell nucleus, cytoplasm, mitochondrion outer membrane, and endoplasmic reticulum (ER) (**Supplemental Fig. S1A**). In differentiated mouse neuro 2A cells (´N2A´ hereafter) (**Supplemental Fig. S1C** and **Methods**), following treatment with the biocompatible and cell-permeable Halo-targetable photocaged electrophile probe [Ht-PreHNE ('REX-probe' hereafter), **Supplemental Fig. S1D**] and washout period,

correct localization of probe-bound Halo was observed for all four instances (**Supplemental Fig. S2**). Following light illumination that rapidly liberates ($t_{1/2\ \text{of photouncaging}}$ < 1 min) the electrophile (here, HNE, or alkyne-functionalized variant, **Supplemental Fig. S1D**) from its photocage, in a space-, time-, and dosage-controlled manner, the resultant effect on global protein synthesis was assessed in N2A cells ectopically expressing established GCE components[10,11] (**Supplemental Fig. S1B** and **S1E**). Initially, we used site-specific incorporation of a bicyclononyne-lysine-derived unnatural amino acid (BCNK)[11] into a specific reporter protein, synthetic HA-tagged actin(K118^{TAG}) to measure changes in translation efficiency (**Supplemental Fig. S1B**). Using either assessment by in-gel fluorescence tracking the Cy5-signal arising from actin(K118)-incorporated BCNK (post Diels-Alder-coupling in cell lysate), or western blot reported by anti-HA-signal corresponding to full-length HA-actin (45 kDa), protein synthesis was only prominently affected when electrophile release occurred in the nucleus, as opposed to other locales (**Figure 1B**-**C**, **Supplemental Fig. S3**). The observed translation suppression was also validated using the whole-proteome GCE-labeling approach[10-12] (**Supplemental Fig. S4**).

Nuclear cap-binding protein subunit 1 (NCBP1) is a first responder; NCBP1-specific electrophile signaling functionally stalls protein translation.

Intrigued by this locale-specific behavior, we proposed that (a) specific nuclear protein target(s) is(are) responsible for propagating this nucleus-specific electrophile-signal to drive translation downregulation. Localis-REX function-guided proximity mapping (**Supplemental Figure S1A**)—when coupled with enrichment proteomics—can quantitively index endogenous locale-specific first-responder proteins[6]. We delivered HNE(alkyne)—an HNE-mimic (**Supplemental Figure S1D**) that can be further modified with biotin using Cu(I)-catalyzed Click chemistry—selectively in the nucleus of N2A cells expressing NLS-Halo. Cells were lysed, treated with biotin-azide in the presence of a Cu(I)-catalyst, precipitated, and then biotinylated proteins were enriched using streptavidin. Following elution, HNE(alkyne)-modified nuclear first-responder proteins were identified using label-free quantification (LFQ)-based proteomics target-ID (**Fig. 1D**, top-row). We note this workflow is different from some of our previous published protocols[5-7,13-17] in which we compared responsivity of nuclear and cytosolic proteins[6]. This difference, and the fact that the cell line used in this instance was different from our previous reports, explains why our previously reported hits were not discovered. The Localis-REX function-guided mapping revealed 6 protein hits, consistently captured across 3 independent biological replicate-runs (**Figure 1D**, **Supplemental Fig. S5**, **Supplemental Table S3**). 3 of 6 (NCBP1, CAND1, and IPO5) represent primarily nuclear residents. We initially chose to focus on these proteins. In all instances, human and mouse proteins of interest (POIs) were highly homologous (**Supplemental**

Fig. S6-S8), so we elected to study the human POIs. The other 3 are annotated to be cytoplasm/ER-associated. Noting also that the ER is in physical continuity with the nucleus[18], the latter 3 proteins may play ´minority´ privileged electrophile sensing at locales distinct from canonical environs—a phenomenon recently unmasked by Localis-REX and often linked to moon-lighting behaviors[6,19,20].

To perform validation of electrophile sensitivity, we used T-REX[13,15], a tool that can rank electrophile sensitivity of specific proteins independent of expression levels (**Fig. 2A**). This electrophile-sensitivity parameter is referred to as ligand occupancy, LO[13,15]. Among the three nuclear-localized candidate POIs, only NCBP1 and IPO5 emerged to be kinetically-privileged[21] electrophile responders (**Figure 2B-C**), although the expression levels of all 3 Halo-fused POIs are largely similar (**Supplemental Fig. S9**). Cand1, which houses 30 cysteines (**Supplmental Fig. S8**), was not electrophile-sensitive under T-REX conditions (**Fig. 2A**), where electrophile is only available transiently and in substoichiometric amounts[13,15]. Notably, the percentage LO of NCBP1 (**Figure 2D**) was on par with the best electrophile-responder proteins we have examined[5-7,13-17,21-25]. Live imaging validated that localization of NCBP1-Halo is chiefly nuclear-restricted as anticipated (**Figure 2E**), consistent with an intrinsic nuclear-localization signal within NCBP1. The LO of IPO5 was more similar to weakly-reactive proteins such as HuR[13,25,26]. These proteins have not always shown phenotypic outputs when labeled by HNE under T-REX.

To evaluate the extent to which the two HNE-sensitive POIs play a role in protein synthesis regulation, we coupled T-REX workflow to GCE-reporter (**Supplemental Fig. S1E**). The resulting T-REX–GCE integrated workflow unveiled that the electrophile labeling of only NCBP1—and not IPO5—modulated protein synthesis (**Figure 2F-G**).

NCBP1 harbors 19 conserved cysteines; yet electrophile-induced translation inhibition was C436-site specific.

We proceeded to identify electrophile-sensitive residues within NCBP1. Although many residues can react with HNE, cysteine is the most intrinsically reactive coded amino acid[4,27], and is most often identified as a kinetically-privileged residue[21]. As an essential large subunit of the nuclear cap-binding complex (CBC), NCBP1 is highly conserved from plants to man (**Supplemental Fig. S10A**). NCBP1 has 19 cysteines that are conserved in human and mouse (**Supplemental Fig. S6** and **S10A-B**), consistent with the overall good conservation of human and mouse proteins[28]. Several of these cysteines are solvent accessible, based on the known single-crystal X-ray structure of human-NCBP1[29] (**Supplemental Fig. S10B**). Each cysteine was individually mutated to alanine. % LO did not change across all single (Cys-to-Ala)-mutants, relative to wild-type (wt) (**Figure 3A**, **Supplemental Fig. S11A**). Mutation of all 19-Cys's to Ala ablated NCBP1's electrophile-sensing propensity (**Figure 3B**,

Supplemental Fig. S11B). All mutants—including the ´all-Cys-to-Ala´ mutant—were soluble and expressed to similar levels as Halo-fusions (**Supplemental Fig. S11C**). Although many proteins we and others have investigated have specific electrophile-sensor cysteines[2-4,27,30], we note that several well-known electrophile-sensor proteins, including Keap1, the prototypical electrophile-sensor protein[31], possess several nucleophilic cysteines.

Having validated that NCBP1 senses electrophiles particularly well, and does so through several of its cysteines, we tested the hypothesis that NCBP1 HNEylation is responsible for translational impairment when HNE is released in the nucleus. GCE assay post-T-REX-assisted electrophile labeling of NCBP1 in cells showed largely similar levels of translation suppression, as we found upon Localis-REX with NLS-Halo (compare **Fig. 1C**, first plot, with **Fig. 2F**, inset). We repeated this experiment with each of the NCBP1 Cys-to-Ala single-point mutants (**Supplemental Fig. S12**). Intriguingly, HNEylation of NCBP1(C436A)-Halo selectively blocked the translation suppression otherwise observed in NCBP1(wt)-Halo, and all the other 18 single-Cys mutants (**Fig. 3C**, **Supplemental Fig. S13**). We further confirmed that the basal level of translation efficiency remained the same in cells, irrespective of expressing either NCBP1(wt)-Halo or NCBP1(C436A)-Halo (**Supplemental Fig. S14**). Thus, although several cysteines can sense electrophiles, only C436 is a functional first-responder residue. We have reported similar situations for CDK9[6], and HSPB7[23] electrophile-sensor proteins, for instance. Importantly, this result validates that translation inhibition observed under T-REX-assisted NCBP1-HNEylation is due to site-specific HNEylation of NCBP1.

To further reinforce our hypothesis that NCBP1-electrophile sensing in the nucleus is a key regulatory axis for protein-synthesis downregulation, we replicated Localis-REX in HEK293T cells co-expressing NLS-Halo and NCBP1(C436A) and assayed for translational efficiency. Compared to parallel cell samples co-transfected with NLS-Halo and empty vector [that balanced plasmid encoding NCBP1(C436A)], overexpression of NCBP1(C436A), strongly, albeit not fully, blocked the translation suppression observed in response to nucleus-specific HNE-buildup in empty-vector control samples under otherwise identical conditions (**Supplemental Fig. S15**). This outcome is consistent with our data, which show that NCBP1 is the main HNE-sensor in the nucleus, and that its labeling at C436 dampens translation. These results further show that other sensors, such as IPO5 (**Fig. 2C-D**), also exist.

Translation suppression induced by NCBP1's electrophile sensing and signal propagation was impervious to NCBP1's canonical binding partners.

NCBP1 partners with NCBP2 to form the CBC that performs numerous context-specific operations in eukaryotic mRNA-biogenesis, mRNA-homeostasis surveillance, and mRNA-translation initiation[32]. The

available structural data of NCBP1–NCBP2 heterodimer, with and without a bound 5′ 7-methylguanosine (m^7G)-cap mimic[29], show that C436 is solvent exposed and distal to the heterodimer interface (**Fig. 3E**, **Supplemental Figure S10D-E**). T-REX on NCPB2-Halo showed electrophile-labeling was not observed on the overexpressed NCBP2; thus, only NCBP1 was privileged first-responder within the CBC (**Supplemental Fig. S16A**). Moreover, HNEylation of NCBP1 suppressed protein synthesis as efficiently when NCBP2 was overexpressed, as in empty-vector-transfected control cells (**Supplemental Fig. S16B**). NCBP1/NCBP2 association was also unperturbed by NCBP1-specific HNEylation (**Supplemental Fig. S16C**).

NCBP1's electrophile signaling regulated cell survival and homeostasis maintenance genes.

NCBP1 is essential for CBC function[32-34]. Given the CBC's crucial roles in RNA maturation, we next investigated the effects of NCBP1-HNEylation on RNA levels using RNA-Seq. NCBP1-HNEylation-induced transcriptomic changes were profiled at three different time-points (3, 6, and 12 h), following T-REX-directed NCBP1-specific HNEylation, against all three technical T-REX controls (light alone, REX-probe alone, and DMSO-vehicle control) (**Supplemental Fig. S17**, **Supplemental Table S4**). Pairwise differential analyses were applied to cells that had undergone NCBP1-specific HNEylation relative to each control (**Supplemental Fig. S18-S20**). Each set was performed in independent biological quadruplicates. The numbers of significantly differentially-expressed (SDE) genes—either up- or downregulated, resulting from each comparative set, are illustrated in Venn diagrams, along with their identities and thresholds (p_{adj}) implemented (**Supplemental Fig. S21**).

STRING analysis[35] of these stringently-selected up- and down-regulated SDEs at each time-point (**Supplemental Fig. S20**) showed that several genes lie outside of known interactions. The outputs from early time-points post NCBP1-specific HNEylation particularly stood out in this regard. Subjecting the same SDE-gene list to *g:Profiler* analysis[36] showed significant enrichment of defined gene ontology (GO)-subterms under biological processes (BPs), and to some extent, molecular functions (MFs) (**Supplemental Fig. S22**) in all time-points. A closer assessment revealed that ~62% (53 out of 86 total) of these top-ranked SDEs are associated with the following (functions): **(i)** transcription factors/coregulators (e.g., *dach1*, *pou3f2*, xbp1, and 10 others); **(ii)** stress/cell-death response (e.g., *txnip*, *hrk*, *bnip3(l)*, *sesn3*, *egln3*, and 15 others); **(iii)** mRNA-biogenesis/translation (e.g., *snrpd3*, *qki*, *tincr*, *mars1*, *yars1*); and **(iv)** receptor–nucleus signal transduction (e.g., *bmp4*, *map2k6*, *cxcr4*, *igfbp5*, and 10 others) (**Supplemental Table S5**). These outputs demonstrate that electrophile modification of NCBP1 has broad-spectrum ramifications on cell homeostasis and survival.

NCBP1(C436)-specific electrophile signaling modulated mRNA-splicing of several genes, including essential transcription factors.

We were further intrigued by the fact that a significant number of our top-ranked SDEs—for instance, 46% (22, out of 48 up- and downregulated SDE-genes) at 12 h time-point (**Supplemental Fig. S20**, **Supplemental Table S5**)—comprised disease-relevant genes that undergo alternative splicing (AS), yielding protein variants with potentially different functions. We opted to preliminarily investigate by qRT-PCR (**Supplemental Table S7**), one such gene, *dach1*—an essential transcription factor in developmental physiology and disease, that was downregulated upon NCBP1-HNEylation (**Fig. 4A**, **Supplemental Fig. S18**). Following T-REX in HEK293T cells ectopically expressing NCBP1-Halo, and consistent with our RNA-Seq results above (**Fig. 4A**, **Supplemental Fig. S18**), qRT-PCR data showed selective depletion of endogenous *dach1* mRNA-transcript, against all controls (**Fig. 4B**, **Supplemental Fig. S23A, Supplemental Table S7**). By contrast, the corresponding abundance of pre-mRNA (assayed using qRT-PCR primers spanning the intronic region flanked by exon-2 and -3), increased upon NCBP1-HNEylation (**Fig. 4C**, **Supplemental Fig. S23B, Supplemental Table S7**). These observations were not due to changes in *dach1* mRNA stability. As expected, the half-life of the corresponding pre-mRNA was short (~2-12 min), and difficult to calculate precisely, although this seemed relatively unperturbed **Supplemental Fig. S24**). These data collectively indicate that *dach1* downregulation induced by NCBP1-HNEylation is likely due to inhibition of splicing.

To independently substantiate the above findings, we built ratiometric-readout-based *dach1*-targeted dual-luciferase reporter systems[25], targeted at an intron of amenable size (intron 10, ~3 kb), flanked by exon-10 and -11. Thus, either an exon-exon sequence (for intron-less reporter), or exon-intron-exon sequence (for intron-10 reporter), from *dach1*-mRNA, was fused upstream of the *firefly* luciferase (ff-Luc) reporter construct, while the *dach1*-3'-UTR was maintained downstream of ff-Luc. Co-expressing this construct alongside a constitutive *Renilla* luciferase (R-Luc) reporter construct in HEK293T cells, we found that NCBP1-HNEylation selectively depleted the intron-10 reporter signal (normalized to R-Luc internal control), while having no effect on the intron-less reporter (**Fig. 4D**). These data further pinpoint the inhibition of splicing at intron-10 induced by NCBP1-HNEylation. Importantly, when we deployed NCBP1(C436A)-Halo in place of the wt-protein, no change in the reporter signal was observed (**Supplemental Fig. S25**).

Beyond its essential transcriptional roles, DACH1 has also been implicated in downregulating cytoplasmic translational programs[37]. We generated *crispr-cas9*-assisted *dach1*-knockout (KO) lines (>90% KO efficiency in both KO lines, **Supplemental Fig. S26A**). Likely linked to DACH1's essential role

in cell growth, KO lines grew significantly slower than the KO-control line, or native HEK293T. Subjecting these lines to T-REX–GCE assay however showed that the same extent of protein-synthesis inhibition was observed across KO-1, KO-2, KO-control, and native cells (**Supplemental Fig. S26B-D**). These data ruled out the functional necessity of DACH1 in explaining NCBP1-HNEylation-induced protein-synthesis stall. In parallel, we also ascertained that NCBP1-HNEylation did not affect the synthetic actin GCE-reporter construct[10,11], at its transcript levels (**Supplemental Fig. S27**)

Transcriptome-wide differential splicing analysis unveiled NCBP1-electrophile signaling elicits multiple alternative splicing events.

Although changes in *dach1* splicing emerged not to be involved in translation downregulation upon NCBP1-HNEylation, these data showed that NCBP1-HNEylation can affect splicing. The CBC indeed binds pre-mRNA-transcripts, post co-transcriptional 5' m^7G-capping[33,34]. It plays several roles in nuclear RNA processing, including regulation of constitutive splicing obligatory for mRNA-maturation[32-34]. Although NCBP1 does not directly interact with the transcript (**Supplemental Fig. S9E**), structural studies hint that its association with NCBP2 is essential for enhancing the latter's affinity to the 5'-cap[29]. The CBC promotes the initial interaction between spliceosome factors and the 5'-end of the pre-mRNA transcript (at the first intron), augmenting spliceosome assembly and splicing[29,33,34]. To examine the extent to which the newly-discovered NCBP1-electrophile signaling affects alternative splicing events, we launched a comprehensive genome-wide differential splicing analysis of our RNA-Seq deep-sequencing datasets. Following the established SUPPA2 pipeline[38] described in **Methods**, we first assigned relative abundances of the splicing events or transcript isoforms [referred to as 'proportion spliced-in (PSI)'[39]] for each transcript identified across all 3 time-points, under 4 different conditions: T-REX (NCBP1-HNEylation), and 3 controls (DMSO-, light-, or probe-alone treatment). The difference in the mean PSI (dPSI) between the two chosen conditions (T-REX vs. designated control) was subsequently derived for each transcript, for each type of alternative events scored, along with associated p_{adj}. Events were grouped accordingly: skipping of exon (SE, including both exon inclusion/exclusion; the most common event in mammals[40]); retention of intron (RI); alternative 5' and 3' splice-site selection (A5SS; A3SS)' and alternative first- and last exon splicing (AF; AL). Hits that fulfill the following requirements: $p \leq 0.05$ and appear under at least 2 pairwise comparisons (i.e., T-REX vs. two different controls), out of the 3, were designated as 'significant events' at each time-point (**Supplemental Table S6**).

Our RNA-Seq data showed AF (44%), followed by SE (20%), A5SS (17%), and A3SS (14%), were the most-preferred alternative events triggered upon NCBP1-HNEylation (**Fig. 4E**). Interestingly, the only report of the CBC influencing AS is associated with the CBC from *Arabidopsis thaliana*[41] (~29% sequence identity to mouse and human NCBP1). *Arabidopsis* CBC affects 101 AS events ($p \leq 0.1$) from the 252 analyzed, with >50% of the AS events being AF[41], likely consistent with the direct positioning of CBC at 5' cap and the first splice site of the pre-mRNA transcript[33,34]. In our survey, among the 1266 transcripts analyzed (where transcript counts were determined using Salmon[42], based on output from RNA-Seq), 200 splicing events, across 119 distinct transcripts, were significantly ($p \leq 0.05$) affected following NCBP1-HNEylation (**Supplemental Table S6**), with respect to controls. For instance, within 6 h following T-REX-enabled NCBP1-HNEylation, *thoc7* (THO Complex subunit 7) that encodes a functional spliceosome-associated protein integral to THO complex involved in mRNA nuclear export, underwent a statistically significant loss of alternative event [skipping-of-exon (SE)] that typically yields mRNA isoform-2 lacking Exon-2 (**Supplemental Fig. S28**). We validated this finding from the transcriptome-wide differential splicing analysis using qRT-PCR. Leveraging primers targeting *thoc7* isoform-2, normalized by results from using primers targeting full-length (isoform-1) (**Supplemental Table S7**), the relative abundance of exon-2-lacking isoform-2 was significantly reduced following T-REX in HEK293T cells expressing NCBP1-Halo, compared to all 3 technical controls (**Supplemental Fig. S29**).

Notably, alternative splicing events of a significant number of genes associated with ribosomal translation were affected by NCBP1-HNEylation, including eukaryotic translation initiation factor 4E-binding protein 1 [4ebp1 (also known as elf4ebp1)]; several ribosomal-subunit proteins, e.g., rpl9, rpl32, and mitochondrial ribosomal-subunit proteins, e.g., mrpl13, mrpl23; and protein that binds hibernating ribosomes (ccdc124) (**Supplemental Table S6**). These findings collectively prompted us to explore potential mechanisms that can explain NCBP1-HNEylation-induced translational suppression through effects on alternative splicing of ribosomal translation-relevant players.

Phosphorylation levels of eIF2α and 4E-BP1 remain unaffected by NCBP1-HNEylation

Given the essential role of CBC in the initiation of 5'-cap-directed translation[32-34], we first explored the key players known to drive translation initiation. Following CBC-dependent translation initiation (CT) and NMD-associated quality control, steady-state translation cycles are driven by eIF4E-dependent 5'-cap-directed translation initiation (ET), as CBC is replaced by eIF4E. However, the functional boundaries between CT vs. ET are becoming increasingly blurred[32-34]. Particularly under stress, the CT-based initiation mechanism is believed to be more operative[33,34]. Nonetheless, both CT- and ET-supported initiation mechanisms require active eIF2α: both are suppressed by phosphorylation of

eIF2α, a global stress-responsive means to rewire translational programs. However, additional stress-reponsive translational remodeling programs are emerging[32-34,43-46]. A major mechanism includes hypophosphorylation of eIF4E-binding protein 1 (4E-BP1), which elicits ET inhibition with minimal effect on CT[33]. This mechanism likely explains heat-shock, late-stage hypoxia, and serum starvation-dependent translational responses, where CT is better able to support the cell translational capacity[32-34,43-46]. We thus assessed the phosphorylation of 4E-BP1 and eIF2α post NCBP1-HNEylation. Neither was changed significantly (**Supplemental Figure S28**).

NCBP1-HNEylation selectively promoted a previously-overlooked alternatively-spliced mRNA isoform, *s6k1-x*

These data led us to zoom into specialized factors unique to CBC-bound mRNA translation. Following splicing, nuclear export of mature mRNAs is accompanied by the CBC, bound at 5'-cap; poly(A)-binding nuclear protein C1 [PABPN(C)1] at 3'-poly(A) tail; and exon-exon junction protein complex (EJC), deposited ~20-24 nts upstream of each exon-exon junction[32-34]. Upregulation of CBC-dependent mRNA-translation is subsequently driven by a series of signaling actions involving activation of mTORC1 that phosphorylates ribosomal protein S6 kinase 1 (S6K1; also known as p70S6K), the resultant activated p-S6K1's recruitment and phosphorylation of SKAR (a component of EJC). Beyond translation initiation and quality control, CBC is emerging to function also in the steady-state translation, particularly during stress[33,34,43-45,47]. We revisited RNA-seq datasets, manually analyzing genes associated with CBC-dependent translation-regulatory pathways. Our RNA-Seq data revealed that *rps6kb1* transcript (encoding protein S6K1) was outstandingly affected following NCBP1-HNEylation: Sashimi plots[48] showed significantly-reduced intronic reads spanning exons 13 and 14; and also exons 12 and 13; but not for the intronic reads spanning upstream exons, such as exons 5 and 6; and exons 6 and 7 (**Figure 5A**).

S6K1 full-length (FL) has several splice variants. The S6K1's alternative, kinase-dead, FL variant, and alternative shorter isoforms arising from alternative events between Exons 6 and 7 (thereby resulting in the loss of Exons 8-15, along with modified/alternative Exon 7), have been studied[49]. The short isoforms from both mouse and human—identical to S6K1-FL up to Exon 6 but missing more than half of the conserved kinase domain—are also considered catalytically-inactive. Interestingly, the short isoforms manifest context-specific oncogenic behaviors, whereas the kinase-dead FL variant is tumor-suppressive[49,50]. By contrast, our analysis (**Figure 5A**) showed that NCBP1-HNEylation functionally impinged on an alternative exon-skipping event distinct from those reported (**Figure 5B**, **Supplemental Fig. S30**). Specifically, the alternative event resulting in S6K1-X (lacking exon 14 and 15;

along with alternatively-spliced intron 12) (**Supplemental Fig. S30**) was suppressed by NCBP1-HNEylation. qPCR analysis of endogenous S6K1, following NCBP1-HNEylation in HEK293T cells, confirmed selective build-up of S6K1-X-associated amplicon that includes part of intron 12 (264 bp), under T-REX, compared to all 3 controls. A significantly-increased ´proportion spliced-in (PSI)[39]´ index was found compared to the amplicon lacking the above-mentioned intron-12 constituent (**Figure 5C**). Both amplicons were further validated by sequencing (**Supplemental Fig. S31-S32**). We proceeded to investigate the functional ramifications of the resulting protein product.

NCBP1-HNEylation selectively produced a truncated S6K1-protein, S6K1-X

EJC constituents, CBC, and poly(A)-binding PABPN(C)1 proteins along with bound mRNA transcripts are exported to the cytoplasm post nuclear mRNA-processing[33,34,51]. These proteins undergo nucleocytoplasmic shuttling and NCBP1-bound mRNA-protein complexes are often coimmunoprecipitated with the EJC components[49,52,53]. We examined the extent to which NCBP1-HNEylation modulates S6K1-FL and S6K1-X at protein levels, and how HNEylated NCBP1 associates with the two S6K1 variants by co-IP. During these experiments, we noticed that following NCBP1-HNEylation, the S6K1-X variant was visibly produced, as early as 2 hours post T-REX-mediated HNEylation. Using the S6K1 antibody that selectively binds N-terminus, this S6K1-X band corresponding to 45 kDa was absent in all control groups, but present in the T-REX groups. As expected, replacing the N-terminal-binding anti-S6K1 antibody with the C-terminal-binding variant manifesting antigenic sequence surrounding alanine at 510, and thus cannot bind S6K1-X lacking the residues: 366-525, did not show the corresponding signal. Moreover, S6K1-X associates with HNEylated NCBP1 more effectively than S6K1-FL (**Figure 5D-E**).

S6K1-short isoform exerted pleiotropic effects on translation.

Given that the level of S6K1-X produced upon NCBP1-HNEylation (10 ± 1%) was modest (**Fig. 5D-E** and **Supplemental Fig. S33A-B**), we posited that S6K1-X would exert a dominant-negative effect on translation. To test this hypothesis, we overexpressed either S6K1-X, or S6K1-FL in HEK293T cells, and compared these effects to cells transfected with an empty vector (EV) control. Consistent with our hypothesis, overexpression of S6K1-X dominantly shut down translation, whereas S6K1-FL had no effect compared to EV control (**Fig. 5F**, **Supplemental Fig. S33C**). Should the effect of NCBP1 HNEylation be mediated through S6K1-X production in cells already expressing this inhibitory splice variant, T-REX to NCBP1 should have minimal effect on translation. In cells expressing S6K1-FL or EV, T-REX-assisted NCBP1-HNEylation caused translation inhibition, as previously observed. However, in

cells expressing S6K1-X, NCBP1 HNEylation had no effect (**Supplemental Fig. S34B**). These outcomes are consistent with the fact that S6K1-X elicits a dominant-negative effect on translation, and that it is a mediator of NCBP1 HNEylation-mediated translation inhibition.

Discussion.

This study presents a previously-unrecognized mechanism to rapidly stall protein synthesis during the build-up of reactive small-molecule stressors in the nucleus. Our data indicate that endogenous electrophilic stress accumulation in the nucleus is predominantly sensed and managed by the large subunit of the CBC, NCBP1, resulting in rapid suppression of global protein synthesis as early as in 2 hours following nuclear-localized electrophile build-up. Such a mode of action is logical, since translation initiation, and associated quality control surveillance mechanisms, constitute the main link between the nucleus and translation[32,52], given that translation is thought to be largely uncoupled from events in the nucleus. These data establish a clear, coordinated response to nuclear electrophilic stress that is strongly distinct from the cytosolic stress response, that martials upregulation of transcription of specific cytoprotective genes. As the nucleus is relatively protected from external reactive small-molecule agents, it is likely that this translation suppression response represents the fact that the build-up of reactive chemicals in the nucleus is mutagenic and potentially highly damaging.

The overall parallels between this mechanism and translation inhibition enacted by ER stress (usually referred to as the unfolded protein response) are not lost on us. In general ER stress responses lead to a general decrease in translation to allow coordinated response to stress. Both also use an unconventional splicing event that helps coordinate the response (S6K1 in the case of nuclear specific stress sensing; XBP1 in the case of ER-stress[54]). However, several factors differentiate our mechanism from traditional stress-response pathways, and highlight the key factors of how substoichiometric electrophile signaling differs from conventional signaling pathways. In our case, NCBP1 is both the initial sensor of electrophile stress and the mediator of differential splicing of S6K1. This mode of the sensor/writer also being the reader is common for reactive small-molecule signaling. In ER stress response, a wealth of protein factors martials translational suppression responses. In the case of NCBP1, its electrophile-labeling leads to a change in splicing, producing a dominant-negative suppressor of translation.

Although the response mode is particularly intriguing and sets new paradigms on how to martial stress, it shoud be noted that our identified electrophile-responder protein is far from being enigmatic. Indeed, NCBP1 emerged to be a sensor of electrophilic stress on par with the best sensors we have characterized. What we did not expect was that none of its cysteines were essential for electrophile

sensing; however, one of its cysteines (C439) was entirely responsible for signaling responses. Given that aberrant translation can play important roles in disease[55-57], and that we have identified a new electrophile-responsive player linked to this process, these data altogether introduce a new privileged sensor ideal for drug target mining[16,58]. Future work will address this aspect, as well as how the other proteins identified in our screen fit into the nuclear electrophile response.

Main Figure legends

Figure 1. Global protein synthesis is most prominently responsive to nuclear-targeted electrophile delivery.

A) Schematic of Localis-REX—GCE integrated platform capable of precision localized electrophile delivery (Localis-REX) and simultaneous readout on protein translation (GCE). A neuronal cell is illustrated as an example. *Top box:* precision perturbation upstream enabled by Localis-REX (see **Supplemental Fig. S1A** for details): the small-molecule electrophilic stressor (red sphere) was liberated rapidly ($t_{1/2}$ < 1 min) upon light illumination (5 mW/cm^2, 365 nm), from the biocompatible photocaged electrophile probe covalently bound to Halo. Halo is expressed in a defined subcellular locale, e.g., nucleus. Limited dosage of electrophile molecules locally available is competed among the best electrophile-sensor proteins within the proximity of Halo. The approach enables kinetically-privileged first responders to be mapped with controls of timing, electrophile chemotype, dosage, and locale. *Lower box:* following localized precision electrophile delivery, genetic code expansion (GCE) method[10,11] reports on precise ramifications of localized electrophilic perturbation on protein synthesis. Note: although this work focuses on 'global translation', tRNA-synthetase can be anchored to a specific locale (e.g., dendrites) to potentially study impacts on 'local translation'. Also see **Supplemental Fig. S1A-B**.

B) Differentiated mouse neuroblasts [neuro-2a (N2A hereafter) cells] ectopically expressing Halo fused to any of the indicated localization sequences [namely, nuclear localization signal (NLS), nuclear export signal (NES), mitochondrial out membrane localization sequence (MOMLS), or ER targeting sequence (ERt)], were subjected to Localis-REX—GCE workflow (see also **Supplemental Table S1-S2**, **Supplemental Fig. S1A-D** and **S2**). Briefly, cells were treated with either DMSO or Ht-PreHNE(alkyne) (10 µM, 2 h). Following washout, the cells were exposed to a hand-held lamp (5 mW/cm^2, 365 nm) allowing rapid delivery of the electrophile, HNE, within a locale designated by the situation of Halo (relevant control samples were kept in dark). Fresh media containing BCNK[11] (50 µM) were next introduced. After 4 h incubation period, cells were lysed, and lysate was treated with Tetrazine-Cy5 (1 µM, 30 min, 37°C) for GCE reporting. In-gel fluorescence (Cy5) and western blot (anti-HA) analyses report the expression level of HA-actin(K118TAG), as a proxy for rates of translation. Anti-tubulin antibody serves as loading control. Also see **Supplemental Fig. S3-S4**.

C) Quantification plots of representative data from **Figure 1B** and **Supplemental Fig. S2**. 'Normalized relative GCE-reporter signal' corresponds to relative values derived from the western blot signal of anti-HA normalized by that of anti-tubulin. P values were calculated with ANOVA and Tukey's multiple comparisons test. All data present mean ±SEM. See **Methods** for sample size information. Also see **Supplemental Fig. S3** for additional replicates.

D) Localis-REX method coupled to LFQ-based quantitative proteomics target-ID workflow for function-guided proximity mapping (*top row*). The six top-ranked kinetically-privileged nuclear-specific electrophile-senor proteins (*table, bottom left*) consistently captured across three independent biological replicates of Localis-REX performed in differentiated mouse N2A cells ectopically expressing nuclear-restricted Halo. Also see **Supplemental Table S3**. The Venn diagram (*bottom right*) shows the number of statistically-significant enriched hits from each replicate. Also see **Supplemental Fig. S5**. Note: the proteins identified are of mouse origins but conserved in humans (see also **Supplemental Fig. S6-S8**).

Figure 2. NCBP1 is a kinetically-privileged electrophile sensor, HNEylation of which downregulates protein translation.

A) T-REX[13,14] precision electrophile-sensor validation workflow: live cells expressing Halo-fused protein of interest (POI) are treated with biocompatible cell-permeable photocaged-electrophile(alkyne-functionalized) probe, followed by washout to remove excess unbound probe. Subsequent light exposure enables rapid ($t_{1/2}$ < 1 min) photouncaging. Providing POI is a kinetically-privileged electrophile sensor (KPS) to the liberated electrophile [HNE(alkyne) herein], the POI is covalently HNEylated, prior to HNE diffusion, which can be quantified by in-gel fluorescence analysis post cell lysis and Click coupling to Cy5-azide (see

Methods and **Supplemental Fig. S1D**). Should POI not be a KPS, the sub-µM amount of HNE transiently made available in the proximity of POI simply diffuses away and is captured by glutathione (5–10 mM), or enzymatically-degraded in the cell[4,21].

B) HEK293T cells ectopically expressing NCBP1-Flag-TEV-Halo (labeled as 'NCBP1-Halo' in figures for brevity) were subjected to T-REX (see **Fig. 2A**), which validated that NCBP1 is a KPS. **Note:** Samples not exposed to light but treated, post-lysis, with TeV-protease that separates NCBP1 and Halo, served as a negative control. Anti-Flag western blot detects the correponding full-length Halo-fusion construct (a remnant from incomplete TeV-cleavage) and NCBP1 post TeV-cleavage. *Indicates NCBP1 post TeV-cleavage (92 kDa). See **Fig. 2D** for quantification.

C) Similar experiments as in **Fig. 2B**. IPO5 (124 kDa, post TeV-cleavage), but not Cand1 (136 kDa, post TeV-cleavage), was validated as a KPS. See **Fig. 2D** for quantification.

D) Quantification of HNE-ligand occupancy (LO) following T-REX KPS validation test on indicated POIs, from **Fig. 2B-C**, using the established T-REX-based LO quantification method[15].

E) Ectopically-expressed NCBP1-Flag-TEV-Halo localizes to the cell nucleus. HEK293T cells transfected with NCBP1-Halo construct (note: NCBP1 from human) were treated with Halo-targetable cell-permeable TMR fluorescent-dye. Following incubation and washout period, the cells were imaged using bright field and TMR-fluorescence (λ_{ex}, 561 nm; λ_{em}, 580 nm) using a Nikon spinning disk confocal microscope. A representative merged image is shown. Scale bar: 10 µm.

F) The validated KPS (NCBP1) was subjected to T-REX coupled to GCE. HEK293T cells were co-transfected with NCBP1-Flag-TEV-Halo, HA-Actin(K118TAG), and tRNA-synthease, MmPylRS (see **Methods** and **Supplemental Fig. S1E**). T-REX was performed followed by BCNK incubation (50 µM, 4 h). Cell lysates were normalized and incubated with 1 µM Tetrazine-Cy5 for 30 min. Both in-gel fluorescence (Cy5) and anti-HA western blot analyses showed translation suppression as reported by selective decrase of bands corresponding to full-length HA-Actin(K118TAG) following T-REX-targeted NCBP1-specific HNEylation, but not during IPO5-HNEylation. P values were calculated with ANOVA and Tukey's multiple comparisons test. All data present mean ±SEM. See **Methods** for sample size information.

G) As in **Fig. 2F** except IPO5-Flag-TEV-Halo was used in place of NCBP1-Flag-TEV-Halo.

Figure 3. The 19 cysteines within NCBP1 play a compensatory HNE-sensing role; only C436-specific HNEylation functionally suppresses protein translation.

A) HEK293T cells ectopically expressing NCBP1-Flag-TEV-Halo (wt, or indicated Cys-to-Ala single-mutant), were subjected to T-REX (**Fig. 2A**) and HNE-ligand occupancy was quantified as prevously reported[13-15], while also taking into account differences in expression levels (if any) as analyzed by anti-Flag western blot. See **Supplemental Fig. S11A** for corresponding in-gel fluorescence (Cy5) and anti-Flag and anti-tubulin western blot analyses. P values were calculated with ANOVA and Tukey's multiple comparisons test.

B) Similar experiment as in **Fig. 3A** was performed except that comparison between wt and all-Cys mutant (the mutant where all 19-Cys's are mutated to Ala) was made. The bands corresponding to HNEylated-NCBP1 post TeV-cleavage (top fluorescence gel) and the corresponding protein (bottom western blot), respectively, were indicated with a red arrow. See also **Supplemental Fig. S11B-C**.

C) Similar T-REX—GCE experiments as in **Fig. 2F** were performed to assess the effect on protein translation in response to T-REX-assisted NCBP1(wt or C436A)-targeted HNEylation. *Inset:* quantification of the results on NCBP1(C436A) against all three T-REX technical negative controls (also see **Supplemental Fig. S11**). See **Fig. 2D** (*inset*) for the corresponding quantification for NCPB1(wt). P values were calculated with ANOVA and Tukey's multiple comparisons test. All data present mean ±SEM. See **Methods** for sample size information.

D) Similar experiment as in **Fig. 3C** was performed for all 18 single-mutants. Also see **Fig. 2D** and **3C**; **Supplemental Fig. S12-S16**. P values were calculated with ANOVA and Tukey's multiple comparisons test. All data present mean ±SEM. See **Methods** for sample size information.

E) 2.00 Å resolution single crystal structure illustrating heterotrimeric complex of NCBP1 and NCBP2 from human (PDB: 1H6K) with C436 in red. (Note: the 3rd molecule of NCBP2 is out of view—hidden behind the NCBP1 molecule in pale magenta). Also see **Supplemental Fig. S10**.

Figure 4. HNEylated NCBP1 modulates mRNA-splicing events.

A) Differental transcript expression from RNA sequencing of HEK293T cells subjected to NCPB1-HNEylation by T-REX against non-treated. (Representative data shown for 3 h time-point post T-REX; see **Supplemental Fig. S17-S20** for schematic workflow and datasets pertaining to additional time-points and additional controls). Statistically-significant differentially-expressed (SDE) genes are marked with **blue** and **red** dots, respectively, for up- and downregulated SDE genes; and non-SDE genes in **grey** dots (also see **Supplemental Table S4-S5** and see, for STRING and *g:Profiler* analyses, **Supplemental Fig. S21-S22**). For the corresponding MA scatter plot featuring fold change vs. mean expression levels, see **Supplemental Fig. S18**.

B) Consistent with RNA-Seq dataset in **Fig. 4A** (DACH1 indicated in red), exon-targeted qRT-PCR analysis in HEK293T cells validated suppression of DACH1 mRNA following T-REX-assisted NCBP1-HNEylation, against all respective T-REX negative controls. P values were calculated with ANOVA and Tukey's multiple comparison test. See **Supplemental Table S7** for primers information; **Supplemental Fig. S23A** for results from primer efficiency tests; and **Supplemental Fig. S24A** for DACH1 mRNA half-life measurement. Also see **Fig. 4C-D** and **Supplemental Fig. S26-S27**.

C) Intron-targeted qRT-PCR analysis in HEK293T cells revealed upregulation of DACH1 pre-mRNA following T-REX-assisted NCBP1-HNEylation, against all respective T-REX negative controls. P values were calculated with ANOVA and Tukey's multiple comparison test. **Supplemental Table S7, Supplemental Fig. S23B** and **S24B** show information on intron-targeting primers, and results from primer efficiency tests, and pre-mRNA half-life measurements, respectively.

D) Results in **Fig. 4B-C** were independently validated by orthogonal reporter assays. Reporters to read out the effect of introns were built by installing the indicated exons within DACH1-mRNA, with or without the intron (left and right, respectively), upstream of a firefly luciferase reporter, with DACH1's 3´-UTR downstream. HEK293T cells ectopically expressing NCBP1(wt)-Halo, intron or intron-less reporter, and CMV-Renilla (internal control plasmid for Renilla luciferase signal for normalization) were subjected to T-REX against indicated controls and Firefly and Renilla luminescence readouts were measured as described in **Methods**. Replicating this assay with NCBP1(C436A) in place of NCBP1(wt) resulted in no change of normalized luciferase signal (see also **Supplemental Fig. S26-S27**).

E) Intron analysis revealed that 200 alternative splicing events across 119 genes were affected (among 1266 genes analyzed in total across 3 h post T-REX datasets, against all negative controls, see **Methods** for details). The relative proportion of these 200 events can be further categorized as: SE, skipping of exon; RI, retained intron; A5(3)SS, alternative 5' (3') splice sites; AF(L), alternative first (last) exon. See **Supplemental Table S6**, and **Supplemental Fig. S28**.

Figure 5. HNEylated NCBP1 generates an alternatively-spliced S6K1 protein that is a phenotypically-dominant inhibitor of protein translation.

A) Representative Sashimi plots[48] (*top*) and quantification derived from Sashimi plots (*bottom*), illustrating the selective reduction in the reads for the S6K1 gene, spanning: exon 12 and 13; exon 13 and 14; following T-REX-assisted NCPB1-HNEylation against DMSO control. This selective decrease was not seen in the reads spanning preceding exons, such as: exon 5 and 6; and exon 6 and 7. P values were calculated with ANOVA and Tukey's multiple comparison test. All data present mean ±SEM. See **Methods** for sample size information. [Note: Sashimi plots are generated using Integrated Genome Viewer (IGV) browser. Genomic coordinates on x-axis are omitted for clarity, and the values within the arcs depict the corresponding raw number of junction reads. For clarity, Sashimi plots are shown for only one representative out of 4

independent biological replicates under two representative conditions, T-REX vs. DMSO. See plots below for quantification of read spans across indicated exons, across all 4 replicate datasets, and under T-REX vs. 3 technical-control groups. FPKM, fragments per kilobase million].

B) Schematic illustration of exon structure of S6K1 pre-mRNA (*top*, E1 to E15, where E indicates exon, and the numbers above individual exons correspond to the no. base-pairs), and the resulting spliced forms: *bottom left*, S6K1-FL mRNA arising from constitutive splicing obligatory for mRNA-maturation; *bottom right*, S6K1-X, an alternative-spliced isoform, S6K1-X, formed as a result of NCBP1-HNEylation (discovered in this work). **Note:** (i) S6K1-X is missing E14 and E15, and partially missing 'E13' due to alternative splicing at intron 12. (ii) The pair of arrows shown for -FL and -X corresponds to the experimental data discussed in **Fig. 5C**. See also **Supplemental Fig. S30**.

C) Following T-REX-enabled NCBP1-HNEylation, amplicon featuring Exon11-Exon12-Exon13 (*bottom band*: 215 bp) and Exon11-Exon12-Intron12-Exon13 (*top band*: 412 bp) were analyzed using primers in **Fig. 5B** (also see **Supplemental Table S7**). PSI: proportion spliced in. Following gel extraction, each band was PCR-amplified and validated by sequencing. See **Supplemental Fig. S30-32**.

D) *Left panel*: Following T-REX-enabled NCBP1-HNEylation in HEK293T cells ectopically expressing NCBP1-Flag-Halo, S6K1-X (45 kDa, red arrow) was selectively generated, as analyzed by western blots using anti-S6K1 and anti-Flag antibodies. *Right panel*: results from subsequent immunoprecipitation workflow using anti-Flag beads (see **Methods** for details). See also **Supplemental Fig. S29** and **S33A-B**.

E) Quantification of the results from **Fig. 5D**: relative ratio of S6K1-X : S6K1-FL in cell lysate versus post IP, normalized by NCBP1-Halo expression. P values were calculated with ANOVA and Tukey's multiple comparisons test. All data present mean ±SEM. See **Methods** for sample size information.

F) S6K1-X (and not S6K1-FL) dominantly suppresses protein translation. HEK293T cells overexpressing S6K1-FL, or S6K1-isoform-X or empty vector (EV), replete with GCE-reporter constructs as described elsewhere, were treated with BCNK (50 µM) for 4 h. Post cell lysis, and coupling with tertrazine-Cy5, the samples were analyzed by in-gel fluorescence (Cy5) reporting protein translation. Western blot analyses were made using anti-V5 tag (reporting the V5 epitope tag in both S6KL constructs), anti-Flag (tRNA synthetase PylRS), and anti-tubulin (loading control) antibodies. (Note: Ectopic expression of S6K1 is known to result in corresponding proteins in two forms, with and without nulcear-localization sequence (NLS), with the latter in greater amount. See **Supplemental Fig. S33C**). NLS-S6K1-FL (74 kDa), S6K1-FL (59 kDa), NLS-S6K1-X (51 kDa), and S6K1-X (45 kDa). *Inset*: quantification. P values were calculated with ANOVA and Tukey's multiple comparison test. All data present mean ±SEM.). See also **Supplemental Fig. S34**.

G) NCBP1(C436)-site-specific electrophilic-stress signaling in the nucleus promotes alternatively-spliced S6K1 that dominantly inhibits global translation.

All full-view blots and gels are shown in **Supplemental Fig. S35-S38.**

Acknowledgements. Drs. Krishna N. Tripathi, Amogh Kulkarni, Kevin T. Fridianto, and Chaosheng Luo (Aye Lab) for the syntheses of Ht-PreHNE, Ht-PreHNE(alkyne), and HNE(alkyne). Mr. Surased Suraritdechachai (Uttamapinant lab), Riyaz Khan (NCCR master thesis student, Aye Lab), and Mr. Tony Hu (ThinkSwiss Scholar, Aye Lab) for assistance with gene cloning. Dr. Chloé Rogg (Aye Lab) for initial training of M.A. and assistance during exploratory investigations. Drs. Romain Hamelin and Maria Pavlou (EPFL proteomics core facility) for assistance with LFQ-DDA differential protecomics data processing and analysis. Drs. Viviane Praz, Hannes Richter, and Julien Marquis (University of Lausanne Genomic Technologies Facility) for assistance with RNA-Seq data processing and analysis. Dr. Ashley Sawle (Principal Bioinformatics Analyst, Cancer Research UK Cambridge Institute) for intron analysis of RNA-Seq data. Research support: Swiss National Science Foundation (SNSF) SPIRIT (grant no. 193915) [to Y.A. (PI) and C.U. (co-PI)]; SNSF R-Equip Funding for proteomics research instrumentation [to Y.A. (PI) and Dr. Maria Pavlou (co-PI)]; and Swiss Federal Institute of Technology Lausanne (EPFL) (to Aye Lab).

Author Contributions. D.C.: performed all experiments, data compilation, analysis, and writing (figure legends and supporting information); M.A.: optimizations toward successful establishment of REX—GCE dual-technology integration; C.S.: collaborated with D.C. in independent validations of REX—GCE dual-technology; K.S.: collaborated with D.C. during initial developments of REX—GCE dual-technology; C.U., SNSF:SPIRIT project grant co-PI: funding acquisition; grant administration; GCE-technology technique transfer, experimental design, and consultation; data analysis; M.J.C.L.: experimental design and data analysis, writing (manuscript critical review and editing); Y.A.: conceptualization, experimental design and data analysis, writing (manuscript draft, critical review, and editing). All authors assisted with final proofing of the manuscript.

Data availability statement. Proteomics data that support the findings of this study (**Fig. 1D, 2B** and **2C Supplemental Table S3**) have been deposited to the ProteomeXchange Consortium via the PRIDE partner repository with the dataset identifier **PXD:051483**. The RNA-seq raw data from this study used to generate **Fig. 4A**, **4E** and **5A, Supplemental Fig. S18-S22, and Supplemental Table S4-S6** have been deposited in the Gene Expression Omnibus (GEO) database under accession code (**GSE:265951**).

Availability of materials. All unique materials will be made available upon reasonable request to the corresponding author.

Competing Interests. The authors declare no conflict of interest.

References.

1 Walsh, C. Posttranslational Modification of Proteins: Expanding Nature's Inventory. (2005).
2 Jacobs, A. T. & Marnett, L. J. Systems Analysis of Protein Modification and Cellular Responses Induced by Electrophile Stress. *Accounts of Chemical Research* **43**, 673-683 (2010).
3 Schopfer, F. J., Cipollina, C. & Freeman, B. A. Formation and signaling actions of electrophilic lipids. *Chemical Reviews* **111**, 5997-6021 (2011).
4 Parvez, S., Long, M. J. C., Poganik, J. R. & Aye, Y. Redox Signaling by Reactive Electrophiles and Oxidants. *Chemical Reviews* **118**, 8798-8888 (2018).
5 Long, M. J. C., Parvez, S., Zhao, Y., Surya, S. L., Wang, Y., Zhang, S. & Aye, Y. Akt3 is a privileged first responder in isozyme-specific electrophile response. *Nature Chemical Biology* **13**, 333-338 (2017).
6 Zhao, Y., Miranda Herrera, P. A., Chang, D., Hamelin, R., Long, M. J. C. & Aye, Y. Function-guided proximity mapping unveils electrophilic-metabolite sensing by proteins not present in their canonical locales. *Proceedings of the National Academy of Sciences* **119**, e2120687119 (2022).
7 Poganik, J. R., Huang, K. T., Parvez, S., Zhao, Y., Raja, S., Long, M. J. C. & Aye, Y. Wdr1 and cofilin are necessary mediators of immune-cell-specific apoptosis triggered by Tecfidera. *Nature Communications* **12**, 5736 (2021).

8 Advani, V. M. & Ivanov, P. Translational Control under Stress: Reshaping the Translatome. *Bioessays* **41**, e1900009 (2019).
9 Pizzinga, M., Harvey, R. F., Garland, G. D., Mordue, R., Dezi, V., Ramakrishna, M., Sfakianos, A., Monti, M., Mulroney, T. E., Poyry, T. & Willis, A. E. The cell stress response: extreme times call for post-transcriptional measures. *Wiley Interdiscip Rev RNA* **11**, e1578 (2020).
10 Chin, J. W. Expanding and reprogramming the genetic code. *Nature* **550**, 53-60 (2017).
11 Uttamapinant, C., Howe, J. D., Lang, K., Beránek, V., Davis, L., Mahesh, M., Barry, N. P. & Chin, J. W. Genetic code expansion enables live-cell and super-resolution imaging of site-specifically labeled cellular proteins. *J Am Chem Soc* **137**, 4602-4605 (2015).
12 Elliott, T. S., Townsley, F. M., Bianco, A., Ernst, R. J., Sachdeva, A., Elsässer, S. J., Davis, L., Lang, K., Pisa, R., Greiss, S., Lilley, K. S. & Chin, J. W. Proteome labeling and protein identification in specific tissues and at specific developmental stages in an animal. *Nature Biotechnology* **32**, 465-472 (2014).
13 Parvez, S., Long, M. J., Lin, H. Y., Zhao, Y., Haegele, J. A., Pham, V. N., Lee, D. K. & Aye, Y. T-REX on-demand redox targeting in live cells. *Nature Protocols* **11**, 2328-2356 (2016).
14 Huang, K. T., Poganik, J. R., Parvez, S., Raja, S., Miller, B., Long, M. J. C., Fetcho, J. R. & Aye, Y. Z-REX: shepherding reactive electrophiles to specific proteins expressed tissue specifically or ubiquitously, and recording the resultant functional electrophile-induced redox responses in larval fish. *Nature Protocols* **18**, 1379-1415 (2023).
15 Long, M. J. C., Rogg, C. & Aye, Y. An Oculus to Profile and Probe Target Engagement In Vivo: How T-REX Was Born and Its Evolution into G-REX. *Accounts of Chemical Research* **54**, 618-631 (2021).
16 Liu, X., Long, M. J. C., Hopkins, B. D., Luo, C., Wang, L. & Aye, Y. Precision Targeting of pten-Null Triple-Negative Breast Tumors Guided by Electrophilic Metabolite Sensing. *ACS Central Science* **6**, 892-902 (2020).
17 Zhao, Y., Long, M. J. C., Wang, Y., Zhang, S. & Aye, Y. Ube2V2 Is a Rosetta Stone Bridging Redox and Ubiquitin Codes, Coordinating DNA Damage Responses. *ACS Central Science* **4**, 246-259 (2018).
18 Cooper, G. M. The Nuclear Envelope and Traffic between the Nucleus and Cytoplasm (The Cell: A Molecular Approach, 2nd edition). (2000).
19 Fu, Y., Long, M. J. C., Wisitpitthaya, S., Inayat, H., Pierpont, T. M., Elsaid, I. M., Bloom, J. C., Ortega, J., Weiss, R. S. & Aye, Y. Nuclear RNR-α antagonizes cell proliferation by directly inhibiting ZRANB3. *Nat Chem Biol* **14**, 943-954 (2018).
20 Jeffery, C. J. Enzymes, pseudoenzymes, and moonlighting proteins: diversity of function in protein superfamilies. *Febs j* **287**, 4141-4149 (2020).
21 Liu, X., Long, M. J. C. & Aye, Y. Proteomics and Beyond: Cell Decision-Making Shaped by Reactive Electrophiles. *Trends Biochem Sci* **44**, 75-89 (2019).
22 Van Hall-Beauvais, A., Poganik, J. R., Huang, K. T., Parvez, S., Zhao, Y., Lin, H. Y., Liu, X., Long, M. J. C. & Aye, Y. Z-REX uncovers a bifurcation in function of Keap1 paralogs. *Elife* **11** (2022).
23 Surya, S. L., Long, M. J. C., Urul, D. A., Zhao, Y., Mercer, E. J., IM, E. I., Evans, T. & Aye, Y. Cardiovascular Small Heat Shock Protein HSPB7 Is a Kinetically Privileged Reactive Electrophilic Species (RES) Sensor. *ACS Chem Biol* **13**, 1824-1831 (2018).
24 Long, M. J., Lin, H. Y., Parvez, S., Zhao, Y., Poganik, J. R., Huang, P. & Aye, Y. β-TrCP1 Is a Vacillatory Regulator of Wnt Signaling. *Cell Chem Biol* **24**, 944-957.e947 (2017).
25 Poganik, J. R., Long, M. J. C., Disare, M. T., Liu, X., Chang, S. H., Hla, T. & Aye, Y. Post-transcriptional regulation of Nrf2-mRNA by the mRNA-binding proteins HuR and AUF1. *FASEB J* **33**, 14636-14652 (2019).
26 Poganik, J. R., Van Hall-Beauvais, A. K., Long, M. J. C., Disare, M. T., Zhao, Y. & Aye, Y. The mRNA-Binding Protein HuR Is a Kinetically-Privileged Electrophile Sensor. *Helvetica Chimica Acta* **103**, e2000041 (2020).
27 Gersch, M., Kreuzer, J. & Sieber, S. A. Electrophilic natural products and their biological targets. *Natural Product Reports* **29**, 659-682 (2012).
28 Breschi, A., Gingeras, T. R. & Guigó, R. Comparative transcriptomics in human and mouse. *Nat Rev Genet* **18**, 425-440 (2017).
29 Calero, G., Wilson, K. F., Ly, T., Rios-Steiner, J. L., Clardy, J. C. & Cerione, R. A. Structural basis of m7GpppG binding to the nuclear cap-binding protein complex. *Nat Struct Biol* **9**, 912-917 (2002).
30 Yang, F. & Wang, C. Profiling of post-translational modifications by chemical and computational proteomics. *Chemical Communications* **56**, 13506-13519 (2020).
31 Dinkova-Kostova, A. T., Hakomäki, H. & Levonen, A. L. Electrophilic metabolites targeting the KEAP1/NRF2 partnership. *Curr Opin Chem Biol* **78**, 102425 (2024).
32 Maquat, L. E., Tarn, W. Y. & Isken, O. The pioneer round of translation: features and functions. *Cell* **142**, 368-374 (2010).
33 Borden, K. L. B. & Volpon, L. The diversity, plasticity, and adaptability of cap-dependent translation initiation and the associated machinery. *RNA Biol* **17**, 1239-1251 (2020).
34 Ryu, I. & Kim, Y. K. Translation initiation mediated by nuclear cap-binding protein complex. *BMB Rep* **50**, 186-193 (2017).
35 Szklarczyk, D., Kirsch, R., Koutrouli, M., Nastou, K., Mehryary, F., Hachilif, R., Gable, A. L., Fang, T., Doncheva, Nadezhda T., Pyysalo, S., Bork, P., Jensen, Lars J. & von Mering, C. The STRING database in 2023: protein–protein association networks and functional enrichment analyses for any sequenced genome of interest. *Nucleic Acids Research* **51**, D638-D646 (2022).

36 Kolberg, L., Raudvere, U., Kuzmin, I., Adler, P., Vilo, J. & Peterson, H. g:Profiler—interoperable web service for functional enrichment analysis and gene identifier mapping (2023 update). *Nucleic Acids Research* **51**, W207-W212 (2023).
37 Wu, K., Chen, K., Wang, C., Jiao, X., Wang, L., Zhou, J., Wang, J., Li, Z., Addya, S., Sorensen, P. H., Lisanti, M. P., Quong, A., Ertel, A. & Pestell, R. G. Cell Fate Factor DACH1 Represses YB-1–Mediated Oncogenic Transcription and Translation. *Cancer Research* **74**, 829-839 (2014).
38 Trincado, J. L., Entizne, J. C., Hysenaj, G., Singh, B., Skalic, M., Elliott, D. J. & Eyras, E. SUPPA2: fast, accurate, and uncertainty-aware differential splicing analysis across multiple conditions. *Genome Biol* **19**, 40 (2018).
39 Schafer, S., Miao, K., Benson, C. C., Heinig, M., Cook, S. A. & Hubner, N. Alternative Splicing Signatures in RNA-seq Data: Percent Spliced in (PSI). *Curr Protoc Hum Genet* **87**, 11.16.11-11.16.14 (2015).
40 Gupta, S., Zink, D., Korn, B., Vingron, M. & Haas, S. A. Genome wide identification and classification of alternative splicing based on EST data. *Bioinformatics* **20**, 2579-2585 (2004).
41 Raczynska, K. D., Simpson, C. G., Ciesiolka, A., Szewc, L., Lewandowska, D., McNicol, J., Szweykowska-Kulinska, Z., Brown, J. W. & Jarmolowski, A. Involvement of the nuclear cap-binding protein complex in alternative splicing in Arabidopsis thaliana. *Nucleic Acids Res* **38**, 265-278 (2010).
42 Patro, R., Duggal, G., Love, M. I., Irizarry, R. A. & Kingsford, C. Salmon provides fast and bias-aware quantification of transcript expression. *Nat Methods* **14**, 417-419 (2017).
43 Daszkowska-Golec, A. Emerging Roles of the Nuclear Cap-Binding Complex in Abiotic Stress Responses *Plant Physiology* **176**, 242-253 (2017).
44 Garre, E., Romero-Santacreu, L., De Clercq, N., Blasco-Angulo, N., Sunnerhagen, P. & Alepuz, P. Yeast mRNA cap-binding protein Cbc1/Sto1 is necessary for the rapid reprogramming of translation after hyperosmotic shock. *Mol Biol Cell* **23**, 137-150 (2012).
45 Koritzinsky, M., Magagnin, M. G., van den Beucken, T., Seigneuric, R., Savelkouls, K., Dostie, J., Pyronnet, S., Kaufman, R. J., Weppler, S. A., Voncken, J. W., Lambin, P., Koumenis, C., Sonenberg, N. & Wouters, B. G. Gene expression during acute and prolonged hypoxia is regulated by distinct mechanisms of translational control. *Embo j* **25**, 1114-1125 (2006).
46 Oh, N., Kim, K. M., Cho, H., Choe, J. & Kim, Y. K. Pioneer round of translation occurs during serum starvation. *Biochem Biophys Res Commun* **362**, 145-151 (2007).
47 Mars, J. C., Ghram, M., Culjkovic-Kraljacic, B. & Borden, K. L. B. The Cap-Binding Complex CBC and the Eukaryotic Translation Factor eIF4E: Co-Conspirators in Cap-Dependent RNA Maturation and Translation. *Cancers (Basel)* **13** (2021).
48 Katz, Y., Wang, E. T., Silterra, J., Schwartz, S., Wong, B., Thorvaldsdóttir, H., Robinson, J. T., Mesirov, J. P., Airoldi, E. M. & Burge, C. B. Quantitative visualization of alternative exon expression from RNA-seq data. *Bioinformatics* **31**, 2400-2402 (2015).
49 Ben-Hur, V., Denichenko, P., Siegfried, Z., Maimon, A., Krainer, A., Davidson, B. & Karni, R. S6K1 alternative splicing modulates its oncogenic activity and regulates mTORC1. *Cell Rep* **3**, 103-115 (2013).
50 Karni, R., de Stanchina, E., Lowe, S. W., Sinha, R., Mu, D. & Krainer, A. R. The gene encoding the splicing factor SF2/ASF is a proto-oncogene. *Nat Struct Mol Biol* **14**, 185-193 (2007).
51 Ma, X. M., Yoon, S. O., Richardson, C. J., Jülich, K. & Blenis, J. SKAR links pre-mRNA splicing to mTOR/S6K1-mediated enhanced translation efficiency of spliced mRNAs. *Cell* **133**, 303-313 (2008).
52 Lejeune, F. & Maquat, L. E. Mechanistic links between nonsense-mediated mRNA decay and pre-mRNA splicing in mammalian cells. *Curr Opin Cell Biol* **17**, 309-315 (2005).
53 Ishigaki, Y., Li, X., Serin, G. & Maquat, L. E. Evidence for a pioneer round of mRNA translation: mRNAs subject to nonsense-mediated decay in mammalian cells are bound by CBP80 and CBP20. *Cell* **106**, 607-617 (2001).
54 Cubillos-Ruiz, J. R., Silberman, P. C., Rutkowski, M. R., Chopra, S., Perales-Puchalt, A., Song, M., Zhang, S., Bettigole, S. E., Gupta, D., Holcomb, K., Ellenson, L. H., Caputo, T., Lee, A. H., Conejo-Garcia, J. R. & Glimcher, L. H. ER Stress Sensor XBP1 Controls Anti-tumor Immunity by Disrupting Dendritic Cell Homeostasis. *Cell* **161**, 1527-1538 (2015).
55 Tahmasebi, S., Khoutorsky, A., Mathews, M. B. & Sonenberg, N. Translation deregulation in human disease. *Nature Reviews Molecular Cell Biology* **19**, 791-807 (2018).
56 Rubio, A., Garland, G. D., Sfakianos, A., Harvey, R. F. & Willis, A. E. Aberrant protein synthesis and cancer development: The role of canonical eukaryotic initiation, elongation and termination factors in tumorigenesis. *Seminars in Cancer Biology* **86**, 151-165 (2022).
57 Khajavi, M., Inoue, K. & Lupski, J. R. Nonsense-mediated mRNA decay modulates clinical outcome of genetic disease. *European Journal of Human Genetics* **14**, 1074-1081 (2006).
58 Long, M. J. C. & Aye, Y. Privileged Electrophile Sensors: A Resource for Covalent Drug Development. *Cell Chem Biol* **24**, 787-800 (2017).

Figure 1

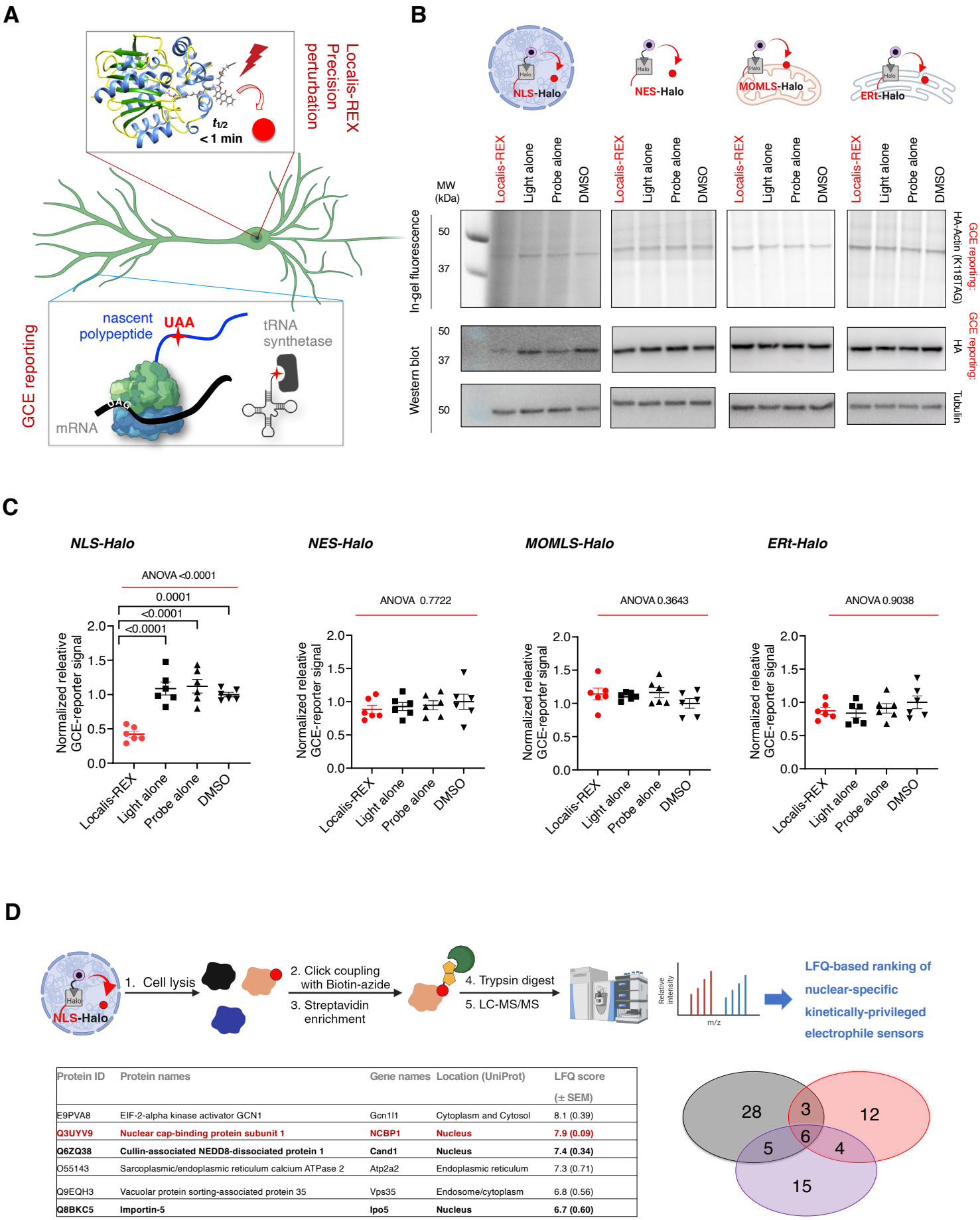

Protein ID	Protein names	Gene names	Location (UniProt)	LFQ score (± SEM)
E9PVA8	EIF-2-alpha kinase activator GCN1	Gcn1l1	Cytoplasm and Cytosol	8.1 (0.39)
Q3UYV9	Nuclear cap-binding protein subunit 1	NCBP1	Nucleus	7.9 (0.09)
Q6ZQ38	**Cullin-associated NEDD8-dissociated protein 1**	**Cand1**	**Nucleus**	**7.4 (0.34)**
O55143	Sarcoplasmic/endoplasmic reticulum calcium ATPase 2	Atp2a2	Endoplasmic reticulum	7.3 (0.71)
Q9EQH3	Vacuolar protein sorting-associated protein 35	Vps35	Endosome/cytoplasm	6.8 (0.56)
Q8BKC5	**Importin-5**	**Ipo5**	**Nucleus**	**6.7 (0.60)**

Figure 2

A

T-REX live-cell-based electrophile-sensor validation workflow:

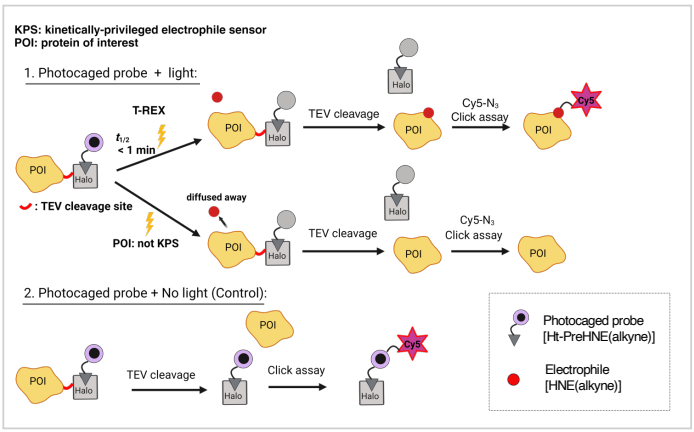

B

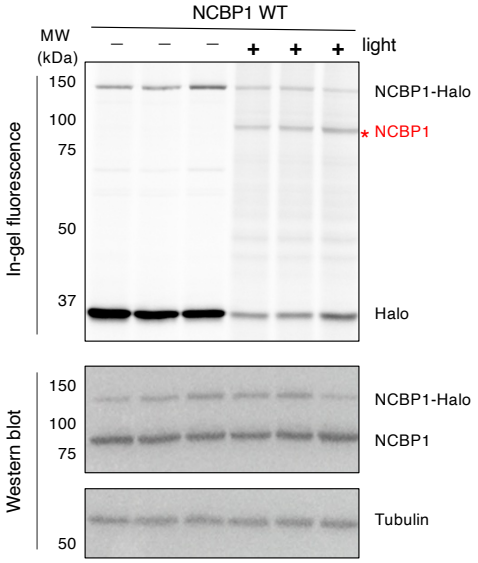

C

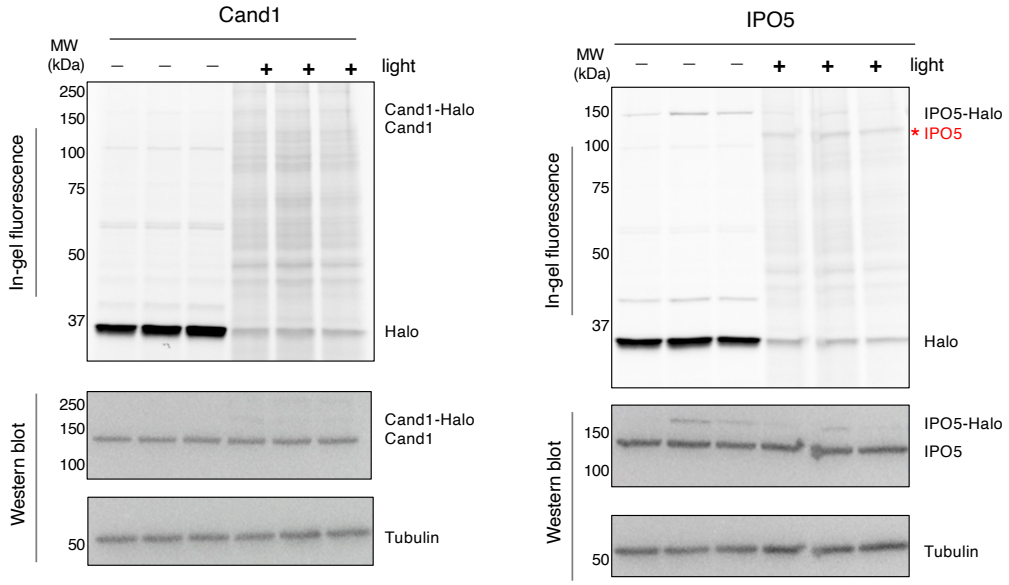

D

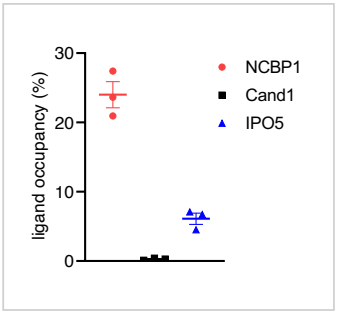

E

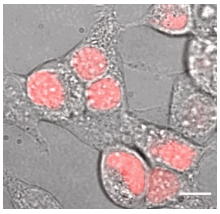

F T-REX (NCBP1) and GCE

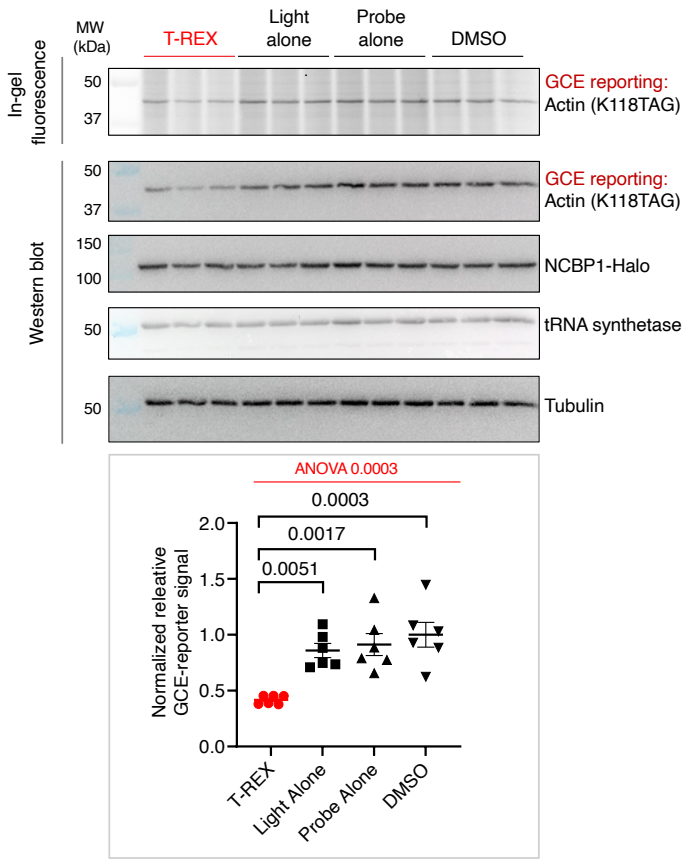

G T-REX (IPO5) and GCE

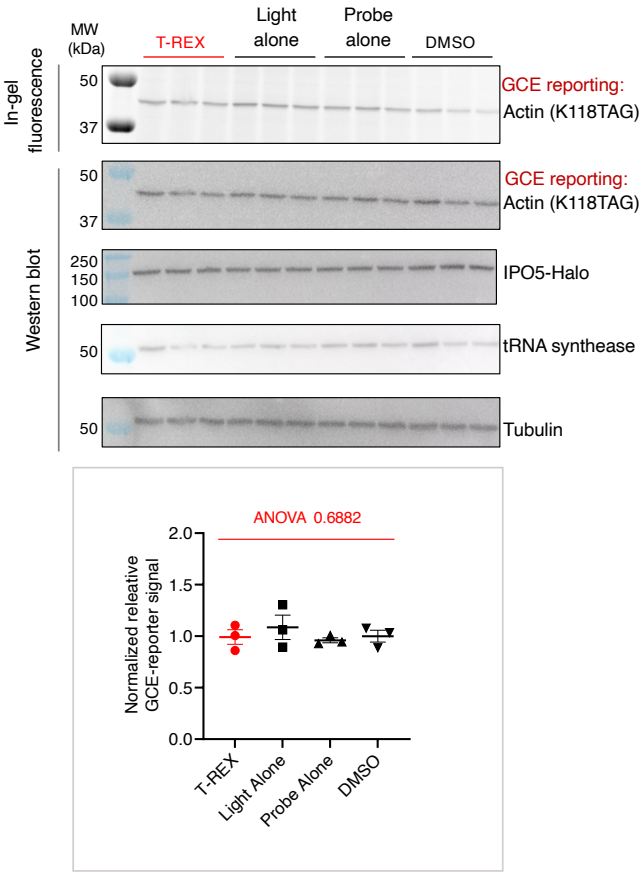

Figure 3

A

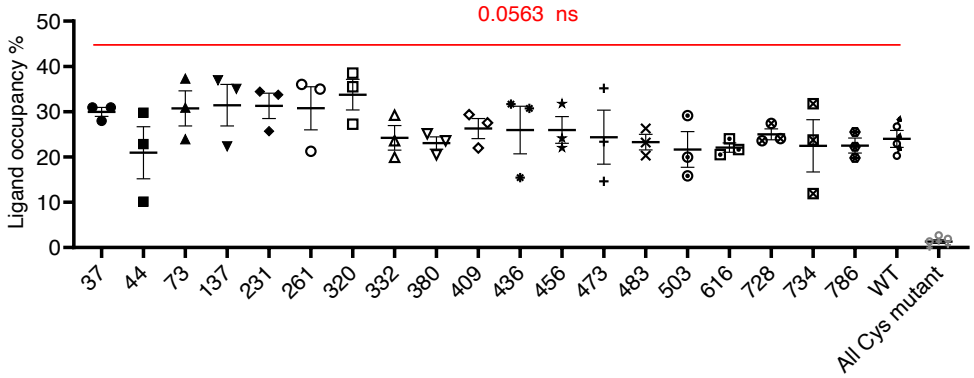

B

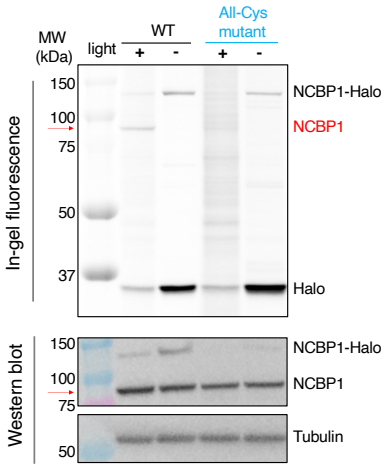

C

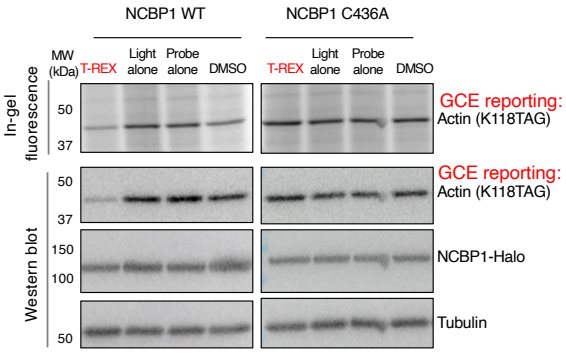

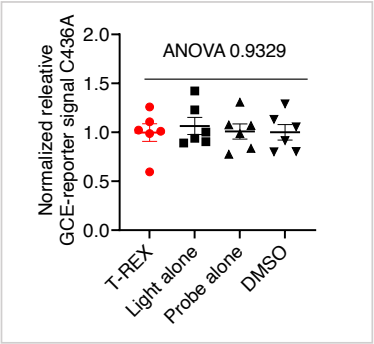

D

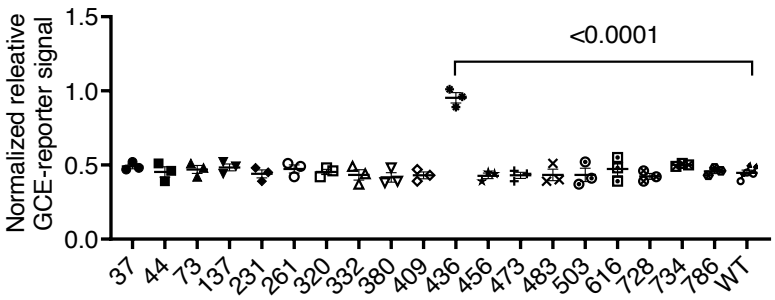

E

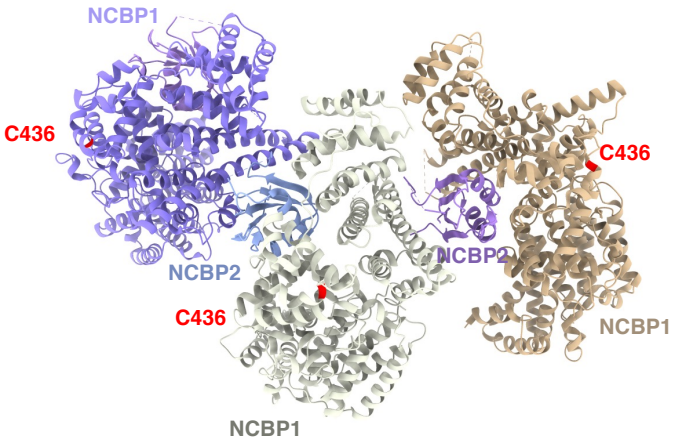

Figure 4

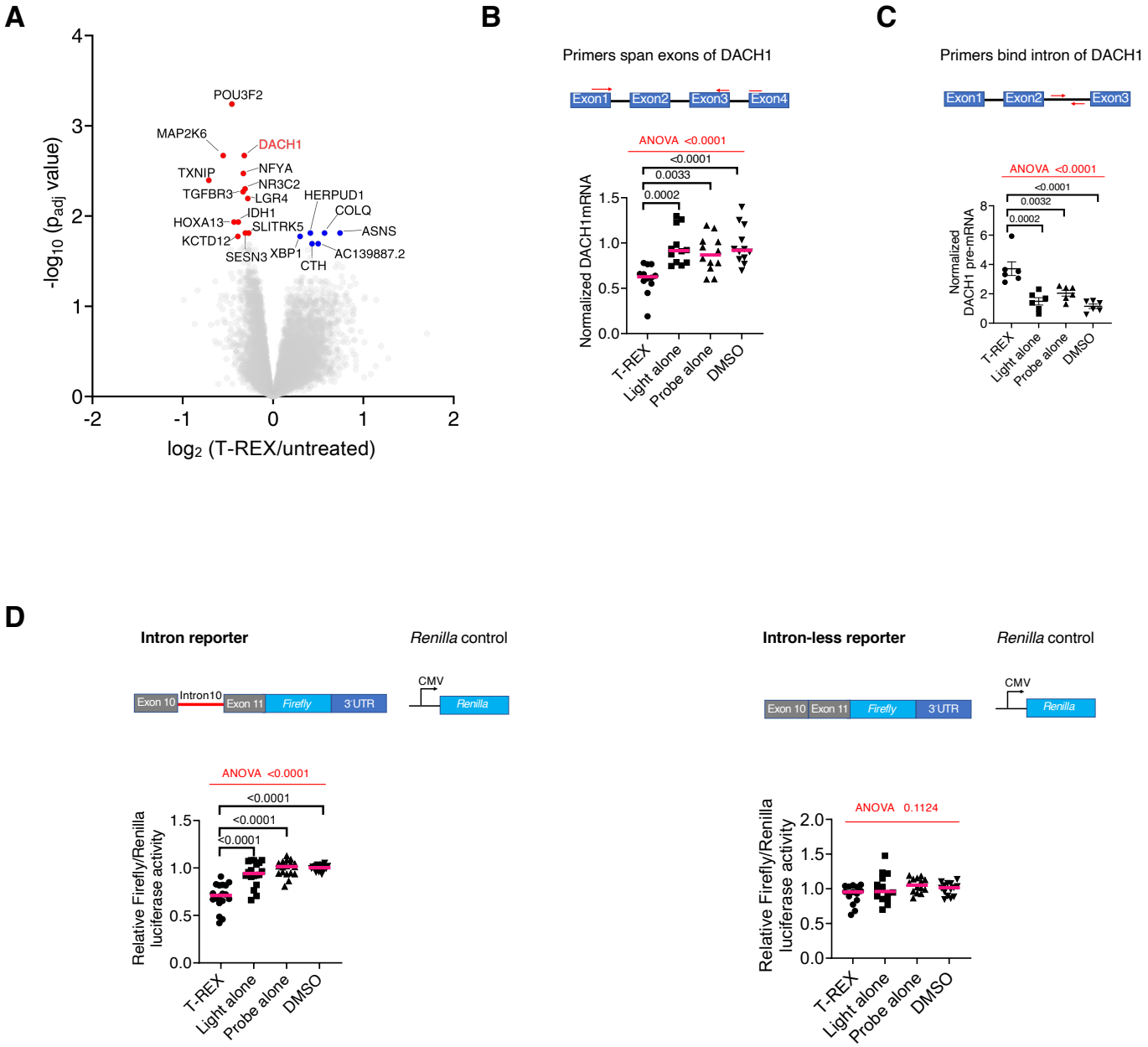
A
POU3F2
MAP2K6
DACH1
TXNIP
NFYA
TGFBR3
NR3C2
LGR4
HERPUD1
IDH1
COLQ
HOXA13
SLITRK5
ASNS
KCTD12
SESN3
XBP1
AC139887.2
CTH
-log10 (padj value)
log2 (T-REX/untreated)
B
Primers span exons of DACH1
Exon1
Exon2
Exon3
Exon4
ANOVA <0.0001
<0.0001
0.0033
0.0002
Normalized DACH1mRNA
T-REX
Light alone
Probe alone
DMSO
C
Primers bind intron of DACH1
Exon1
Exon2
Exon3
ANOVA <0.0001
<0.0001
0.0032
0.0002
Normalized DACH1 pre-mRNA
T-REX
Light alone
Probe alone
DMSO
D
Intron reporter
Renilla control
Exon 10
Intron10
Exon 11
Firefly
3'UTR
CMV
Renilla
ANOVA <0.0001
<0.0001
<0.0001
<0.0001
Relative Firefly/Renilla luciferase activity
T-REX
Light alone
Probe alone
DMSO
Intron-less reporter
Renilla control
Exon 10
Exon 11
Firefly
3'UTR
CMV
Renilla
ANOVA 0.1124
Relative Firefly/Renilla luciferase activity
T-REX
Light alone
Probe alone
DMSO
E
20%
14%
17%
44%
SE
RI
A3SS
A5SS
AF
AL

Figure 5

A

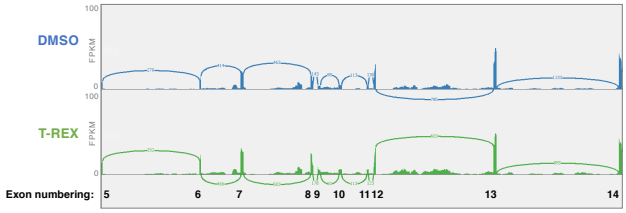

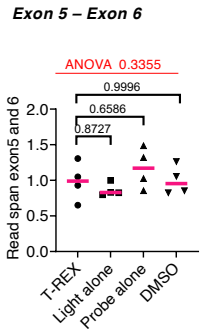

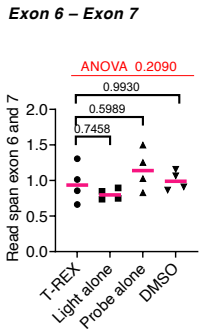

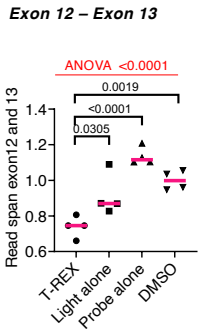

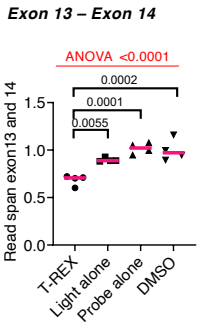

B

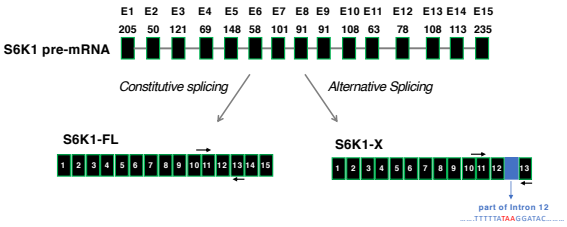

D

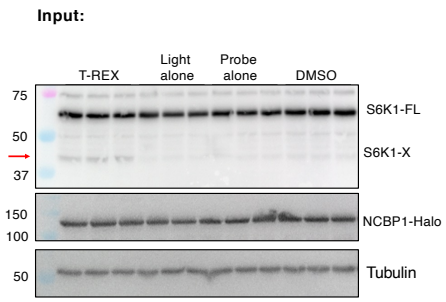

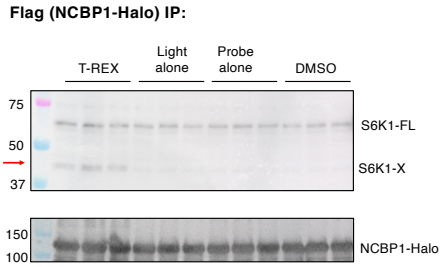

C

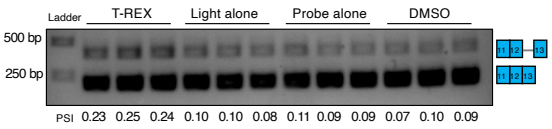

E

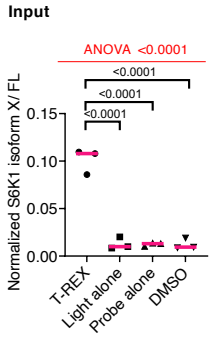

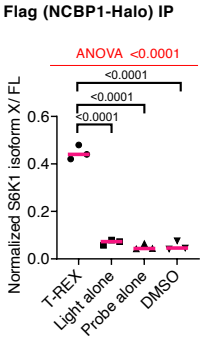

F

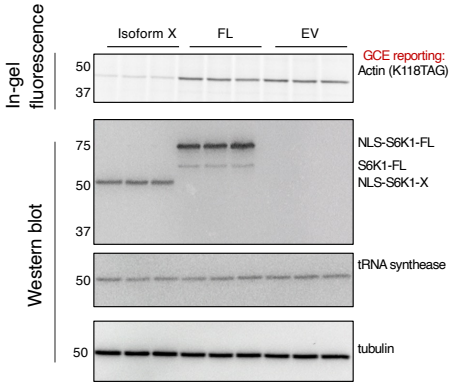

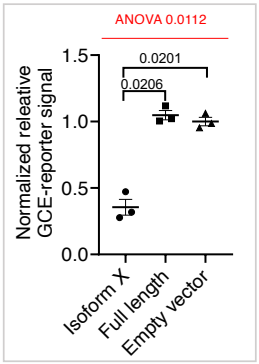
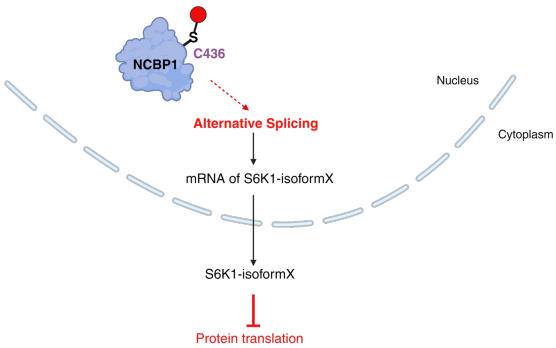
G